Analytical Potentials for HF Dimer and Larger HF Clusters from ab Initio Calculations

Matthew P. Hodges and Anthony J. Stone*

University Chemical Laboratory, Lensfield Road, Cambridge CB2 1EW, U.K.

Enrique Cabaleiro Lago

Departamento de Química Física, Facultade de Química, Universidade de Santiago, Avenida das ciencias s/n 15706, Santiago de Compostela, Spain

Received: July 2, 1997; In Final Form: December 1, 1997

A new ab initio potential for hydrogen fluoride dimer is presented, constructed from properties calculated for the monomer and intermolecular perturbation theory calculations on the dimer. The potential is split into clearly defined contributions. The long-range electrostatic energy is represented by a distributed multipole model with multipoles up to hexadecapole. The induction energy is modelled by means of polarizabilities up to rank 2 at the center of mass. The repulsion energy is described by an anisotropic exponential site−site model. For the dispersion, two models have been used: a one-site anisotropic and a two-site isotropic model, both incorporating damping functions. The geometries, binding energies, and barrier height to tunneling motion are in good agreement with previous calculations. We also compare the classical and quantum corrected second virial coefficient with the limited data available. The potential is extended to larger clusters, the induction energy accounting for many-body contributions to the energy. For the trimer to the hexamer, we have characterized minima and transition states and decomposed the total interaction energy into its *n*-body components.

1. Introduction

Hydrogen fluoride dimer has been the subject of numerous experimental and theoretical studies. It is, like water, a strongly hydrogen-bonded system, dominated by the electrostatic interaction. Owing to its small size and few degrees of freedom, this system is very suitable for accurate spectroscopic and ab initio studies. As a result of the spectroscopic studies[1−12] very accurate structural parameters, dissociation energies, and several fundamental vibrational frequencies are available. There have been extensive theoretical studies of the HF dimer,[13−26] many of which focus on the determination of structure and energy at the equilibrium geometry. More extensive calculations were presented by Bunker et al. in a series of papers.[20−24] They computed the energy of the dimer at a very large number of different geometries using the averaged coupled pair functional theory (ACPF), and fitted the results to an analytic function, which they used to calculate the lowest intermolecular vibration levels. Since this work, other similar calculations have been carried out.[11,27−29]

Over the last few years, considerable computational effort has been concentrated on the HF dimer, notably the work of Peterson and Dunning[13]—high-level supermolecule calculations, up to CCSD(T) level using correlation consistent basis sets,[30] and extrapolated to the complete basis set limit to obtain properties of the ground state of $(HF)_2$ very accurately—and a six-dimensional ab initio HF dimer potential,[11] which is probably the most accurate to date. We also refer the reader to a recent paper by Quack and Suhm[31] for a concise summary of theoretical and experimental results obtained for HF dimer.

The theoretical ab initio description of intermolecular interactions is usually calculated using either the supermolecule method,[32,33] where the interaction energy is obtained as the difference between the energy of the whole system and the energy of the isolated molecules, or by the perturbation method,[34] where the interaction energy is obtained directly as a sum of several contributions. Both methods have their advantages and their limitations. The supermolecule method is very simple to use, but can be sensitive to basis set superposition error (BSSE), although the counterpoise correction[35] is usually employed to reduce this. With increasing computational power, larger basis sets can be used, and BSSE becomes less of a problem. More importantly, the supermolecule method yields only the total interaction energy, and gives little insight into the nature and characteristics of the interaction. In the perturbation approach, the different terms of the interaction energy can easily be related to monomer properties, especially at long range, where the overlap between the wavefunctions of the monomers is negligible. At short range, the perturbation approach needs to take into account this overlap of the charge distribution of the monomers, and the antisymmetry of the dimer wavefunction. These problems have been solved at the SCF level by Hayes and Stone[36,37] and more recently at the correlated level by Jeziorski et al.[34]

In this paper, we describe our attempts to build accurate intermolecular potential functions for HF dimer and apply them to larger HF clusters. These potential functions were constructed by performing ab initio intermolecular perturbation theory calculations on the dimer for a number of configurations and by fitting the results to suitable analytic functions. We have included anisotropy by means of a distributed multipole model of the electrostatic energy, using multipoles up to the hexadecapole at the atoms and the center of the bond, and by using an anisotropic site−site model for the repulsion. We have also included polarizable sites at the atoms with polarizabilities up

* Author to whom correspondence should be addressed.

S1089-5639(97)02148-8 CCC: $15.00
Published on Web 03/19/1998

TABLE 1: Calculated Monomer Properties for HF at SCF and MP2 Correlated Level at the Experimental Geometry (R = 1.7325)[70] [a]

	SCF	MP2	CI-SD[73]	exptl
energy	−100.05502	−100.28059		
μ	0.7565	0.6854	0.7079	0.7093[b]
θ	1.74	1.70	1.73	1.75[c]
Ω	2.58	2.40	2.45	
Φ	4.99	4.66	4.74	
$\alpha_\perp$	5.74	6.42	6.33	6.59[b,d]
$\alpha_\parallel$	4.46	5.38	5.09	5.10[d,e]

[a] All quantities in atomic units. The electric quadrupole, octupole, and hexadecapole are defined with respect to the center of mass. [b] Reference 71. [c] Reference 72. [d] Reference 107. [e] Reference 108.

to quadrupole−quadrupole. We have used two alternative formulations for the dispersion: an anisotropic one-site model and an isotropic two-site model. It is found, as observed in previous cases,[38−40] that including the anisotropy improves the quality of the potential function significantly.

Redington reported second virial coeflficient data[41,42] some years ago and compared a number of model potentials,[43−48] concluding that the best available at the time was that due to Klein et al.[45] This was used by Redington in the determination of ring and chain structures for larger clusters up to the octamer. Since this time other potentials have been proposed, the most interesting to us, because of the treatment of many-body terms in the energy, being the "(1 + 2 + 3)-body" potential of Quack, Stohner, and Suhm.[49] This was used in the study of clusters up to the heptamer. Also of interest is work by Dykstra[19] using a rigid-body model potential comprising an electrostatic component and a simplistic term describing the "shape" of the molecules, which encompasses all other contributions to the binding energy. This scheme, molecular mechanics for clusters (MMC), is well suited for application to very large systems because of the simple functional forms used.

Previous work has concentrated mostly on ringlike structures[50−53] or chains,[52,54,55] whereas we have undertaken extensive searches of the potential energy surfaces for transition states and minima in an effort to find potentially important tunneling motions.

2. Method

The potential surface presented here was constructed from calculated monomer electrostatic properties and from IMPT[36,37] calculations at more than a hundred different configurations of the dimer. From these calculations we obtain the first-order terms (exchange-repulsion and electrostatic energy) and the single excitation second-order terms (polarization and charge-transfer). We have found that the basis sets provided by Sadlej[56] are very suitable for our purposes. After trying several basis sets, we have concluded that the Sadlej basis sets provide a good balance between size and quality of the monomer properties, especially polarizabilities. Some calculated monomer properties are shown in Table 1 at the SCF and Møller−Plesset[57] (MP2) levels of theory. The MP2 correction of electrostatic properties brings them into good agreement with experiment, especially the dipole moments and the dipole−dipole polarizabilities. The bond lengths are not very good, but our principal aim was to reproduce the electrostatic properties.

In the dimer calculations, the monomer bond length was fixed at the experimental value. A grid of 1372 dimer geometries was chosen, using Gauss−Legendre integration points in α and β, and equally spaced values of ϕ, the torsion angle, and R (see Figure 1). About 125 IMPT calculations were performed at

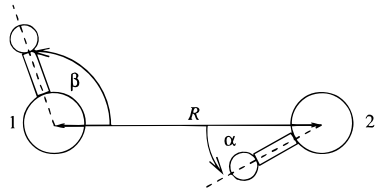

Figure 1. Minimum energy HF dimer geometry. The structure is planar (C_s symmetry). Molecule 1 is the proton acceptor and molecule 2 is the proton donor.

configurations of the dimer chosen randomly from this grid and a number of linear geometries were added. The interaction energy may be expressed as

$$E_{\text{tot}} = E_{\text{es}} + E_{\text{er}} + E_{\text{ind}} + E_{\text{ct}} + E_{\text{disp}} \tag{1}$$

of which the first four terms are provided by the IMPT calculation. E_{es} is the multipolar electrostatic interaction, E_{er} is the exchange−repulsion together with the penetration part of the electrostatic interaction, E_{ind} the induction energy, and E_{ct} the charge-transfer energy. The charge-transfer term is formally part of the induction energy, but it is possible to separate it in a well-defined way[58] and it is more conveniently treated separately because it decays exponentially with distance and so has to be described by a different analytic function from the induction term. Each of these individual terms was described by a suitable functional form. All the ab initio calculations were performed using the CADPAC program,[59] which includes the IMPT program[36,37] and the distributed multipole analysis procedure.[60,61]

A different treatment was used in modelling the dispersion term. It can be calculated using the IMPT method, which in effect gives the dispersion energy at the MP2 level of theory, but better calculations have been carried out by Wormer and his colleagues, and we have used their dispersion coefficients.[62−64] At short range it is necessary to damp both the induction and dispersion terms, and we have used conventional Tang−Toennies damping functions for this purpose.[65]

All geometry optimizations were performed using the ORIENT3.2 program,[66] incorporating analytic second derivatives of the energy and using the eigenvector following (EF) technique of Cerjan and Miller[67] as refined by Wales.[68]

2.1. Electrostatic Energy. The electrostatic energy obtained from IMPT theory is the Coulombic interaction energy between the charge distributions of the two molecules. It can be accurately represented by means of a distributed multipole expansion for any configuration where the molecular charge distributions do not overlap significantly. The electrostatic energy at long range can then be expressed in the form

$$E_{\text{es}} = \sum_{a\in A}\sum_{b\in B} Q_t^a\, T_{tu}^{ab}\, Q_u^b \tag{2}$$

where t and u are labels for the multipole moments and T_{tu}^{ab} is an interaction function which depends upon the distance between the two sites a and b and on the relative orientation of the two molecules. Expressions for these interaction functions have been tabulated previously.[60,69]

We have calculated the distributed multipoles at the experimental geometry[70] using (8s6p3d1f/6s3p1d) basis sets with three sites, situated on the two atoms and at the centre of the bond. The local electric multipoles up to rank 4 are shown, in spherical tensor notation, in Tables 2 and 3, at SCF and MP2 correlated level, and the overall molecular moments are also shown,

TABLE 2: Nonzero Components of the Electric Multipoles for HF at SCF Level[a]

	fluorine ($z =$ −0.087 276)	center of bond ($z =$ 0.778 981)	hydrogen ($z =$ 1.645 239)	total multipoles (origin at $z = 0$)
Q_{00}	−0.062 023	0.092 699	−0.030 675	
Q_{10}	0.416 001	−0.004 418	0.317 755	0.756 494
Q_{20}	0.493 822	0.396 548	−0.087 045	1.742 142
Q_{30}	−0.107 597	−0.201 287	0.027 893	2.575 823
Q_{40}	−0.241 909	0.128 731	−0.005 843	4.987 806

[a] In atomic units. The origin is at the center of mass.

TABLE 3: Nonzero Components of the Electric Multipoles for HF at MP2 Level[a]

	fluorine ($z =$ −0.087 276)	center of bond ($z =$ 0.778 981)	hydrogen ($z =$ 1.645 239)	total multipoles (origin at $z = 0$)
Q_{00}	−0.096 093	0.239 690	−0.143 603	
Q_{10}	0.339 674	0.038 870	0.348 021	0.685 410
Q_{20}	0.511 308	0.371 787	−0.086 102	1.699 428
Q_{30}	0.079 971	−0.228 008	0.023 389	2.403 863
Q_{40}	0.229 440	0.131 259	-0.003 537	4.656 429

[a] In atomic units. The origin is at the center of mass.

relative to a local axis system in which the molecular axis is the z axis, and the origin is at the center of mass.

Comparing with the experimental data available for the molecular properties (Table 1),[71,72] we see that the MP2 results generally constitute an improvement over SCF, the exception being the quadrupole. We also make comparisons with other ab initio calculations due to Amos.[73] At MP2, both the octopole and hexadecapole moments appear to be slightly too small.

When the molecules do overlap there is a penetration contribution which is not described by the multipolar expansion. This is defined here as the difference between the IMPT electrostatic energy and the electrostatic energy obtained with the multipole expansion. That is,

$$E_{\text{pen}} = E_{\text{es}}(\text{IMPT}) - E_{\text{es}}(\text{DMA}) \tag{3}$$

When calculating the penetration energy, the DMA electrostatic energy must be calculated with the SCF multipoles for consistency with the IMPT approach, and using the same basis. In this way we can obtain the SCF penetration energy.

2.2. Exchange−Repulsion and Penetration Energy. The exchange−repulsion energy contains two contributions: the exchange energy, arising from the exchange of electrons between different molecules, and the repulsion energy, reflecting the fact that electrons with the same spin cannot occupy the same region of space. The exchange−repulsion energy is repulsive, and decays almost exponentially with separation. We have also absorbed into this term the penetration energy, which for moderate overlap is attractive and decays in an exponential way. We can obtain the overall contribution by subtracting the SCF electrostatic energy as predicted by the multipolar model, from the IMPT first-order energy, which is the sum of the exchange−repulsion and electrostatic energies. We have fitted this overall contribution to an exponential function of the form:

$$E_{\text{rep}} = C \sum_{a \in A} \sum_{b \in B} \exp\{-\alpha_{ab}(\Omega_{ab})[R_{ab} - \rho_{ab}(\Omega_{ab})]\} \tag{4}$$

where R_{ab} is the distance between the sites a and b in molecules A and B respectively. ρ_{ab} is a function of relative orientation describing the effective shape of the sites in the molecule, and α_{ab} describes the hardness of the repulsion, which may also depend on the relative orientation of the sites. C is a constant with units of energy, and in our case has been chosen to be equal to 1 mhartree, which is about 2.6 kJ mol^{-1}. The orientational dependence of α and ρ is expressed as a linear combination of the $\bar{S}$ functions developed by Stone et al.[74,75]

$$\rho^{ab}(\Omega_{ab}) = \sum_{l_a l_b j} \rho^{ab}_{l_a l_b j} \bar{S}_{l_a l_b j}(\omega_a, \omega_b, \omega_{ab}) \tag{5}$$

$$\alpha^{ab}(\Omega_{ab}) = \sum_{l_a l_b j} \alpha^{ab}_{l_a l_b j} \bar{S}_{l_a l_b j}(\omega_a, \omega_b, \omega_{ab}) \tag{6}$$

In these formulae, ω_a is a set of Euler angles defining the orientation of site a and ω_b similarly, while ω_{ab} is a set of Euler angles specifying the orientation of the intersite vector from site a to site b. Ω_{ab} is an abbreviation for the set (ω_a, ω_b, ω_{ab}).

Using this model, we have explored several different sets of expansion functions, and have obtained the results presented in Table 4. In all the fits we have minimized the Boltzmann-weighted sum of squares, using a Boltzmann weighting factor exp ($-E/kT$) with $kT = 2.5$ mhartree, corresponding to $T =$ 790 K. It can be seen from the table that the inclusion of the anisotropy in the model greatly improves the quality of the fit. The inclusion of three more terms in each expansion reduces the root-mean-square error by a factor of about 10. From the results obtained with different fits, we have found that the addition of further terms in the expansion has little effect on the error and that anisotropy in α has quite a big effect on the quality of the fit.

TABLE 4: Parameters for the Exchange−Repulsion−Penetration Energy of HF[a]

Isotropic Site Model (RMS[b] Error 195.5 μE_h)			
α^{FF}_{00}	2.5578	ρ^{FF}_{00}	5.3268
α^{FH}_{00}	1.9643	ρ^{FH}_{00}	4.1145
α^{HH}_{00}	1.3672	ρ^{FH}_{00}	3.8363
Anisotropic Site Model (RMS[b] Error 21.19 μE_h)			
α^{FF}_{00}	2.5351	ρ^{FF}_{00}	5.3306
α^{FF}_{10}	−0.2308	ρ^{FF}_{10}	0.1400
α^{FF}_{20}	−0.0382	ρ^{FF}_{20}	0.0376
α^{FF}_{30}	0.3448	ρ^{FF}_{30}	−0.0126
α^{FH}_{00}	1.9494	ρ^{FH}_{00}	4.1211
α^{FH}_{01}	0.7090	ρ^{FH}_{01}	−0.0823
α^{FH}_{10}	0.7924	ρ^{FH}_{10}	0.0697
α^{FH}_{02}	0.1849	ρ^{FH}_{02}	0.0290
α^{FH}_{20}	0.3718	ρ^{FH}_{20}	0.0547
α^{FH}_{03}	−0.2597	ρ^{FH}_{03}	−0.0629
α^{FH}_{30}	−0.2479	ρ^{FH}_{30}	0.1382
α^{HH}_{00}	1.4589	ρ^{HH}_{00}	3.8317
α^{HH}_{10}	0.2143	ρ^{HH}_{10}	−0.4395
α^{HH}_{20}	−0.0642	ρ^{HH}_{20}	0.0842
α^{HH}_{30}	−0.2108	ρ^{HH}_{30}	0.0089

[a] In a_0^{-1} and ρ in a_0. The local z axis for both F and H is taken in the direction from F to H. [b] RMS = root mean square.

2.3. Dispersion Energy. The dispersion energy is an important contribution to the binding energy for HF clusters, so we need to model it as accurately as possible. It can be calculated using IMPT, and that procedure takes into account the exchange effects (damping) appropriately, but the results are not very accurate since IMPT does not treat electron repulsion in a self-consistent way, and the effects of intramolecular correlation are not included in the dispersion. We have chosen to use the dispersion surfaces provided by Rijks and Wormer[62,63] and Hettema,[64] who have calculated accurate dispersion coefficients from polarizabilities at imaginary

TABLE 5: Dispersion Coefficients[a] $C_n(l_a, l_b, j)$ for HF[62,63]

n	l_a	l_b	j	$C_n(l_a, l_b, j)$	n	l_a	l_b	j	$C_n(l_a, l_b, j)$
6	0	0	0	20.4777	8	3	1	4	8.2582
6	2	0	2	1.4002	8	1	3	4	8.2582
6	0	2	2	1.4002	8	2	2	4	8.0386
6	2	2	4	0.3138					
					9	1	0	1	676.6772
7	1	0	1	25.8304	9	0	1	1	676.6772
7	0	1	1	25.8304	9	3	0	3	375.3372
7	3	0	3	6.5023	9	0	3	3	375.3372
7	0	3	3	6.5023	9	2	1	3	101.3619
7	3	2	5	1.7044	9	1	2	3	101.3619
7	2	3	5	1.7044					
7	2	1	3	1.4792	10	0	0	0	8984.9797
7	1	2	3	1.4792	10	2	0	2	2074.0830
					10	0	2	2	2074.0830
8	0	0	0	389.9699	10	1	1	2	996.2124
8	2	0	2	78.7833	10	4	0	4	850.4311
8	0	2	2	78.7833	10	0	4	4	850.4311
8	1	1	2	30.0207	10	3	1	4	557.9433
8	4	0	4	18.8990	10	1	3	4	557.9433
8	0	4	4	18.8990	10	2	2	4	367.4311
8	1	1	0	−9.3815	10	1	1	0	348.6743

[a] Coefficients in atomic units.

frequencies using very large basis sets with a correlated zeroth-order wave function within the framework of many body perturbation theory. In this way, the long-range dispersion energy can be expressed as

$$E_{\text{disp}} = -\sum_{n=6}^{10} \sum_{l_a l_b j} C_n(l_a, l_b, j) \bar{S}_{l_a l_b j}(\omega_a, \omega_b, \omega_{ab}) R^{-n} \quad (7)$$

The coefficients we have used in the parameterization of the dispersion energy are given in Table 5. We have not used all the coefficients provided in the literature, because the complexity of the $\bar{S}$ functions increases with their rank, and the use of the complete set of coefficients would complicate the calculation of the potential. The neglected coefficients are small, and the truncation of the expansion has little effect in the region of interest near the minimum; the biggest contribution we have discarded accounts for about 0.08 kJ mol^{-1} to the total energy at 5 a_0.

Though Wormer's coefficients are probably the most accurate way to represent the dispersion energy, they only hold at long range. At short range, we must take exchange effects into account, to avoid the singularity in eq 7 at $R = 0$. This is usually accomplished using damping functions, obtained empirically or from calculations on atoms. We have used Tang−Toennies[65] damping functions, which are incomplete gamma functions:

$$f_n(R) = 1 - e^{-aR} \sum_{k=0}^{n} \frac{(aR)^k}{k!} \quad (8)$$

so the dispersion energy finally is

$$E_{\text{disp}} = -\sum_{n=6}^{10} \sum_{l_a l_b j} C_n(l_a, l_b, j) \bar{S}_{l_a l_b j}(\omega_a, \omega_b, \omega_{ab}) f_n(R) R^{-n} \quad (9)$$

It is necessary to assign a value to the a parameter in the damping function. The quantity aR can be regarded as a measure of the overlap of the wavefunctions of the two molecules, and therefore it should correspond to the exponent in the repulsion energy or to a related magnitude. Following this approach, we first adopted damping factors equal to the hardness parameters obtained from a fit of the exchange−repulsion−penetration energy with an isotropic model and only one site situated on the center of mass. The value we obtained was 2.26 a_0^{-1}. The weakness of this treatment is the model for the damping, and more specifically, its anisotropy. Tang−Toennies damping functions are justified for closed-shell atoms, but in a molecular environment, the overlap will depend very strongly on the orientation, and so should the damping function. Unfortunately, there is no clear way at present to accomplish this. For this reason, we have also implemented another model for the dispersion: an isotropic two-site model, in which the dispersion energy is expressed as

$$E_{\text{disp}} = -\sum_{a \in A} \sum_{b \in B} C_6^{ab} R_{ab}^{-6} f_6^{ab}(R_{ab}) \quad (10)$$

TABLE 6: C_6 Parameters[76] Used in the Isotropic Atom−Atom Dispersion Potential[a]

F−F	F−H	H−H
10.24	4.64	2.1

[a] Parameters in atomic units.

TABLE 7: One-Site Polarizabilities for HF Molecule. $\alpha_{l_a\kappa_a l_b\kappa_b} = \alpha_{l_b\kappa_b l_a\kappa_a}$[a]

l_a	κ_a	l_b	κ_b	$\alpha_{l_a\kappa_a l_b\kappa_b}$	l_a	κ_a	l_b	κ_b	$\alpha_{l_a\kappa_a l_b\kappa_b}$
1	0	1	0	5.740	2	0	2	0	20.052
1	1c	1	1c	4.456	2	1c	2	1c	12.255
1	1s	1	1s	4.456	2	1s	2	1s	12.255
1	0	2	0	3.916	2	2c	2	2c	8.143
1	1c	2	1c	0.768	2	2s	2	2s	8.143
1	1s	2	1s	0.768					

[a] Polarizabilities in atomic units. In the parameterization the dipole−dipole polarizabilities were replaced by the experimental values, and the others were increased by 25%.

The parameters for this isotropic atom-atom model[76] are given in Table 6. We do not expect this to be very accurate, but it does introduce more anisotropy into the damping. In fact, it is in better agreement with the IMPT results than the anisotropic one-site model, particularly for smaller F−F separations.

We note that the damping factors provided from the fit of the repulsion are not satisfactory, and we have adjusted them by comparison with the IMPT dispersion results, which take account of the overlap of the charge distributions at short range.

2.4. Induction Energy. The induction energy describes the response of the charge distribution of a molecule when distorted by an external field. To deal with this contribution to the energy we have used a one-site model, carrying polarizabilities up to rank 2. In the light of previous calculations on water[38] we do not expect that a two-site model with polarizabilities distributed over the atoms will improve the results. Table 7 shows the nonzero components of the polarizability up to rank 2 in spherical tensor notation. These are SCF polarizabilities, because at the moment we have no easy way of calculating MP2 polarizabilities other than the dipole−dipole ones. For this reason, as well as to try to correct part of the error due to the incompleteness of the basis set, we have replaced the dipole−dipole polarizabilities by their experimental values and increased the other polarizabilities by 25%.

In spherical tensor notation $\alpha_{l_a\kappa_a l_b\kappa_b}$ describes the response of the rank $l_a\kappa_a$ multipole to the $l_b\kappa_b$ derivative of the electric potential and vice versa. The calculation of the induction energy and the validity of the multipolar approach have been discussed before,[77,78] so they will not be treated here. As in the case of the dispersion, this model for the induction needs to be damped

TABLE 8: Parameters Used in the Representation of the Charge-Transfer Term in HF Dimer

α_{00}^{FF}	2.4964	ρ_{00}^{FF}	3.8525
α_{10}^{FF}	−0.1155	ρ_{10}^{FF}	−0.0649
α_{20}^{FF}	−0.3602	ρ_{20}^{FF}	−0.2410
α_{30}^{FF}	−0.3125	ρ_{30}^{FF}	−0.1487
α_{00}^{FH}	2.0813	ρ_{00}^{FH}	3.1622
α_{01}^{FH}	0.1115	ρ_{01}^{FH}	−0.0487
α_{10}^{FH}	−0.1738	ρ_{10}^{FH}	0 0009
α_{02}^{FH}	−0.4785	ρ_{02}^{FH}	0.2443
α_{20}^{FH}	0.0919	ρ_{20}^{FH}	−0.1282
α_{03}^{FH}	0.4162	ρ_{03}^{FH}	−0.2003
α_{30}^{FH}	−0.1562	ρ_{30}^{FH}	0.0106
α_{00}^{HH}	1.6747	ρ_{00}^{HH}	2.1758
α_{10}^{HH}	0.1387	ρ_{10}^{HH}	0.1385
α_{20}^{HH}	−0.2022	ρ_{20}^{HH}	−0.5095
α_{30}^{HH}	0.1739	ρ_{30}^{HH}	0.3569

to take account of the exchange effect at short range. We have implemented the same Tang−Toennies damping functions that were used in modelling the dispersion, but in this case, we have followed a different procedure to obtain a value for the damping factor *a*, using the results obtained for the polarization energy from the IMPT calculations as a guide to the parameterization. In this way we have compared the SCF induction energy obtained from the model with the results from IMPT calculation, and after some trial and error we have arrived at a value for the *a* parameter of 1.64 a_0^{-1}.

An important problem in the evaluation of the induction energy is the determination of induced moments.[77,78] To calculate the induced moments on one site, it is necessary to know the potential and its derivatives at the site, but this depends on the induced moments of the other molecules. This problem is usually solved by an iterative procedure. We have found that iteration of the induced moments usually improves the results, but only by a few percent, while the computational time is increased by a factor of 2 or 3 for the dimer, and by more for the larger clusters.

Another contribution to the energy closely related to induction is charge transfer. This term is really part of the induction energy, but it can be calculated separately and it makes quite an important contribution to the energy near the minimum. We have represented it using the same model as for the repulsion, but as it is attractive the preexponential constant *C* is set to −0.001 hartree. The parameters used are shown in Table 8.

2.5. Many-Body Energy. The importance of many-body terms in the energy has been studied by us for small water clusters[79] following work by Xantheas,[80,81] and we refer the reader to these articles for a detailed account of the methodology. However, we note that, for our potentials, the many-body terms in the energy are mediated by the induction contribution, all other terms being pairwise additive, and that we cannot account for fragment relaxation[82] with our rigid-body monomers. Studies of nonadditive effects[83,84] show that induction dominates in polar systems, and we have neglected other nonadditive terms. The use of damping functions in the induction interactions models the exchange part of the induction interaction. A previous study of water clusters[85] compared the Axilrod−Teller triple−dipole[86] and the induction contributions, concluding that the latter was dominant. The nonadditivity in the charge-transfer term appears to be small.[87]

The characterization of reaction pathways for the trimer to the hexamer was first performed on potential energy surfaces for which the induction energy was not converged. For the complete many-body information, the induction energy must be iterated to convergence and we first optimize the geometries on the corresponding potential energy surfaces which typically takes fewer than 10 steps. All dimer results include full iteration of the induction energy.

TABLE 9: Comparison with Selected Previous Calculations on $(HF)_2$. Equilibrium binding Energies and Geometries. Values in Parentheses are BSSE Corrected. For the ASP Potentials, the Induction Energy Is Iterated to Convergence

ref	method	E_{tot} (kJ mol^{-1})	$R(a_0)$	α (degrees)	β (degrees)
this work	ASP	−17.249	5.2716	7.7	108.4
this work	ASP-id	−18.897	5.1775	5.7	109.7
17	SQSBDE	−18.7	5.20	8	115
11	MP2[a]	−18.82	5.19	6.0	112.4
		(−17.80	5.23	6.4	112.2)
	MP2/R12[b]	−19.12	5.17	8.2	112.8
13	MP4	−19.765 (−18.577)	5.1684	6.5	110.4
	CCSD(T)	−19.765 (−18.769)	5.1627	6.7	110.8
24	CPF	−18.075	5.2759	6.8	114.5
21	ACPF	−18.117	5.2478	6.8	114.4
25	MP4	−20.753	5.2232	5.5	112
2	exptl	−19.4(7)[c]	5.14(6)	10(6)	117(6)

[a] V_{MP2} and V_{MP2-CP} ab initio surfaces. [b] SC-2.9 surface, which has been empirically refined. [c] D_e, estimated[7,10] from a value of D_0 = 12.70(1) kJ mol^{-1}.

TABLE 10: Comparison with Selected Previous Calculations on $(HF)_2$. Vibrationally Averaged Binding Energies and Geometries. For the ASP potentials, the Induction Energy Is Iterated to Convergence

ref	method	D_0 (kJ mol^{-1})	$R(a_0)$	α(degrees)	β(degrees)
this work	ASP	−10.22(1)	5.35(2)	22.0(6)	116(1)
this work	ASP-id	−11.04(1)	5.29(2)	19.0(5)	116(1)
17	SQSBDE	−12.64			
11	MP2/R12[a]	−12.69			
2	exptl	−12.70(1)	5.25		

[a] SC-2.9 surface, which has been empirically refined.

3. Results

In this section we present the results obtained with our model potentials for some of the characteristic features of the potential surface of HF dimer, before examining larger HF clusters. It is known that the dimer minimum corresponds to a "classical" hydrogen-bonded complex, controlled mostly by the electrostatic interaction. One of the principal purposes of a potential surface is to reproduce the experimental geometry and energy of the minimum. However, this task is quite difficult, owing to the flatness of the potential surface near the minimum, especially with respect to the angular variables. In the following sections, ASP (anisotropic site potential) will denote the model with the anisotropic one-site dispersion and ASP-id the model with isotropic atom−atom dispersion.

3.1. Dimer. *3.1.1. Stationary Points.* There is general agreement that the equilibrium structure for the dimer corresponds to the one presented in Figure 1, with $\alpha \approx 10°$ and $\beta \approx 120°$. Geometries and energies calculated with our anisotropic site−site potentials are given in Table 9. Our equilibrium results are in quite good agreement with other ab initio calculations e.g., those of Peterson and Dunning[13] and Klopper, Quack and Suhm,[11] and the experimental results (which include a back-correction for the vibrational averaging). The torsion angle is not presented in Tables 9−11 but its value is 0° for all of the stationary points. The experimental dissociation energy has been determined to be 12.70 kJ mol^{-1}. Our values of D_0 from diffusion Monte Carlo (DMC) calculations are smaller in

TABLE 11: Energy Decomposition and Geometries for Several Stationary Points on the $(HF)_2$ Potential Surface. Induction Energy Is Iterated to Convergence[a]

	R	α	β	E_{tot}	E_{es}	E_{rep}	E_{ind}	E_{disp}	E_{ct}
					ASP				
C_s	5.2716	7.7	108.4	−17.25	−19.30	12.15	−3.67	−5.02	−1.41
C_{2h}	5.0616	52.6	52.6	−14.33	−17.61	11.86	−1.93	−5.72	−0.92
$C_{\infty v}$	5.5833	0.0	180.0	−11.96	−10.74	4.65	−2.09	−3.30	−0.49
					ASP-id				
C_s	5.1775	5.7	109.7	−18.90	−20.70	15.16	−4.23	−7.40	−1.72
C_{2h}	5.0371	51.3	51.3	−14.69	−18.15	13.03	−2.08	−6.43	−1.06
$C_{\infty v}$	5.4654	0.0	180.0	−12.99	−11.20	6.14	−2.42	−4.89	−0.62
					CPF[b]				
C_s	5.2759	6.8	114.5	−18.08					
C_{2h}	5.2837	54.2	54.2	−13.81					
$C_{\infty v}$	5.4626	0.0	180.0	−14.02					

[a] Energies in kJ mol^{-1}. R in bohr. Angles in degrees. [b] Reference 24.

magnitude than experiment, as are our values of D_e, estimated from experimental data[7,10] to be −19.4(7) kJ mol^{-1}, but the comparison of zero-point energies is reasonably good (Table 10). Of the two potentials, ASP-id is in better agreement with experiment and high level ab initio results regarding the binding energy.

Another important feature of the $(HF)_2$ potential energy surface is the existence of two equivalent minima and the possibility of tunneling from one to the other. Therefore, it is important to characterize the saddle points and to determine the barrier heights. Both models predict the expected C_{2h} saddle point with barriers of 2.92 and 4.21 kJ mol^{-1} for ASP and ASP-id, respectively. The value for ASP-id compares well with values calculated by Kofranek et al.[24] (4.27 kJ mol^{-1}) and Klopper et al.[11] (4.2(2) kJ mol^{-1}). For ASP, the problem is not with the transition state but with the minimum. It can be seen that the energies and geometries at the the transition state are rather similar for ASP and ASP-id, but for ASP the minimum is not bound strongly enough and this seems to be attributable to underestimation of the dispersion energy at this configuration. The deficiency of the dispersion surface for ASP is that the damping is not anisotropic. Comparison with IMPT shows that at the minimum the dispersion energy is too small, whereas at the transition state and the $C_{\infty v}$ linear stationary point, the results are more consistent. For ASP-id, the comparison is good at all three of these stationary points. A complete decomposition of the energy is given in Table 11 for the minimum, transition state, and $C_{\infty v}$ stationary point, which has Hessian index 2. The experimental tunneling splitting can be measured to very high accuracy.[9,88] This property of the potential energy surface is of course highly sensitive to both the height and width of the tunneling barrier making it a challenging property to reproduce accurately. From the DMC calculations performed, ASP gave a value of 2.8 cm^{-1} and ASP-id 1.7 cm^{-1}, compared with the experimental value of 0.66 cm^{-1}. The larger value found with ASP is primarily attributable to the smaller barrier height for the rearrangement.

3.1.2. Second Virial Coefficient. The second (pressure) virial coefficient, here denoted $B(T)$, is a global property of the potential energy surface and importantly depends strictly only on pairwise interactions. We consider both the classical contributions $B_{cl}(T)$ and the quantum corrections $B_{qu}(T)$ (translational and rotational), to first order in $\hbar^2$ (see for example Gray and Gubbins[89]) according to

$$B(T) = B_{cl}(T) + B_{qu}(T)$$

$$= B_{cl}(T) + B_{qu}^{tr}(T) + B_{qu}^{rot}(T) \quad (11)$$

where

$$B_{cl}(T) = -\frac{1}{2}\int \langle \exp(-U/kT) - 1\rangle_{\omega_1\omega_2}\, d\mathbf{r} \quad (12)$$

$$B_{qu}^{tr}(T) = \frac{\hbar^2}{24(kT)^3}\left[\frac{\langle \mathbf{F}^2\rangle_0}{M}\right] \quad (13)$$

$$B_{qu}^{rot}(T) = \frac{\hbar^2}{24(kT)^3}\left[\sum_\alpha \frac{\langle T_\alpha^2\rangle_0}{I_{\alpha\alpha}}\right] \quad (14)$$

Here U is the pair potential energy; ω_1 and ω_2 the Euler angles describing the orientation of each molecule; **F** the force exerted on each molecule and T_α the torque about the local principal axis α, for which the moment of inertia is $I_{\alpha\alpha}$. Redington[41] used thermodynamic properties over a very narrow temperature range (292.5−329 K) to acquire an estimate of $B(T)$, and we are not aware of any other experimental data. We are cautious in comparing our results with those of Redington because the data were fitted using a fairly simple functional form and are therefore unlikely to be reliable over the temperature range for which we have obtained results. Also, in Redington's fitting procedure the parameters were chosen so that the curve in the high-temperature regime matched that calculated using the potential due to Klein et al.[45] (KMO). Our results (both classical and quantum corrected) for ASP and ASP-id are shown in Figure 2, alongside those from the KMO potential and Bosanac et al.[90] (BBM). We see large discrepancies between our results and those of Redington, especially at low temperature, but note that ASP potentials developed for water have been very successful in reproducing the reliable experimental values of $B(T)$[91−94] over a large range of temperatures.[38,95]

We present the breakdown of the contributions to $B(T)$ in Table 12. ASP-id is more strongly bound at the minimum than ASP, and it is in better agreement with recent ab initio calculations. We therefore expect these results to be more reliable. At 293.15 K (just above the boiling point of HF) the quantum corrections to $B(T)$ for ASP-id are about 35% as large as the classical contribution, but of the opposite sign. At the highest temperature, this ratio is about 6%. As we have found for water,[95] the corrections from the rotational degrees of freedom are about an order of magnitude larger than those from the translational degrees of freedom, and as for water, this is because the molecular moment of inertia is small.

3.2. Trimer−Hexamer. For the study of the larger clusters, we have used only the ASP-id potential on account of its greater success at reproducing the HF dimer potential energy surface. Furthermore, we use only a first-order approximation of the induction energy for the characterization of the pathways.

3.2.1 Minima. We have searched for minimum-energy structures of $(HF)_n$ clusters using periodic quenching of Monte Carlo simulations. The energies of all the minima found are listed in Table 13, along with their point groups and descriptions. In these calculations, the induction was included to first order only. Some of the lower-lying minima are collected in Figure 3. The lowest energy minimum found for each of the clusters $(HF)_3$ to $(HF)_6$ is cyclic. The dimer global minimum has already been discussed—we note that the C_{2h} symmetry dimer transition state can be thought of as cyclic. Table 14 shows a comparison of the energies of the ASP-id cyclic minima (with fully iterated induction) with other results from the literature. It can be seen

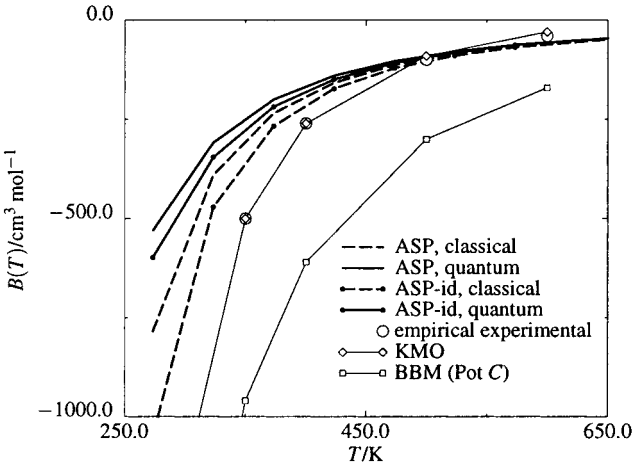

Figure 2. Second virial coefficient for HF: results from "experiment" (Redington[41,42]) and model potentials [KMO (Klein, McDonald, and O'Shea[45]) and BBM (Bosanac, Brobjer, and Murrell[90])].

TABLE 12: Second Virial Coefficient Calculated from the two-model Potentials

	ASP				ASP-id			
T/K	B_{cl}	B^{tr}_{qu}	B^{rot}_{qu}	B	B_{cl}	B^{tr}_{qu}	B^{rot}_{qu}	B
273.15	−784.71	29.71	226.16	−528.84	−1049.30	38.80	412.97	−597.51
293.15	−574.84	17.06	137.52	−420.26	−732.98	21.21	235.89	−475.87
323.15	−389.53	8.36	72.80	−308.37	−470.67	9.81	115.80	−345.06
373.15	−234.38	3.21	31.24	−199.93	−266.79	3.52	45.35	−217.91
423.15	−157.63	1.52	16.12	−139.99	−172.69	1.59	21.96	−149.14
473.15	−113.61	0.83	9.41	−103.37	−121.21	0.84	12.26	−108.10
523.15	−85.72	0.50	6.01	−79.21	−89.65	0.50	7.57	−81.58
573.15	−66.74	0.32	4.09	−62.32	−68.69	0.32	5.02	−63.35
673.15	−42.96	0.16	2.18	−40.62	−43.08	0.16	2.58	−40.34
773.15	−28.92	0.10	1.31	−27.51	−28.33	0.09	1.52	−26.71
873.15	−19.79	0.06	0.86	−18.86	−18.90	0.06	0.98	−17.85
973.15	−13.45	0.04	0.60	−12.80	−12.43	0.04	0.68	−11.71

[a] All components in $cm^3\ mol^{-1}$.

that there is good agreement with previous rigid-body results.[19] The binding energies are smaller than the ab initio results, though the fraction recovered remains quite consistent for the trimer to the pentamer.

All the higher energy minima which we have found are based on one of the cyclic minima or the dimer minimum. For example, we have found just two minima for the trimer; the lower in energy is the C_{3h} cyclic structure as reported in numerous previous studies;[41,49,50,96,97] the less strongly bound has C_{2v} symmetry and has already been described by Quack et al.[49] It is based on the dimer equilibrium geometry, with the central HF molecule acting as proton acceptor to the other two symmetrically displaced HF fragments. All the other structures, except for 6g, comprise a cyclic unit containing three or more HF molecules, with additional HF molecules attached to the ring either as proton donors or proton acceptors. Structure 6g, the exception, has two cyclic trimers arranged in a trigonal antiprism (or distorted octahedron). Such "sandwich" structures, and their importance, have been discussed elsewhere.[98] The minima can be described with a simple labelling scheme based on the principal cyclic (or dimer) unit present and the arrangement of additional HF molecules about it. Each *n*-molecule cyclic unit is denoted by *n*. Additional groups in (or near to) the plane are denoted as n_{md} or n_{ma} for a chain of length *m* acting as proton donor or proton acceptor respectively (*m* omitted for $m = 1$). A group of *m* molecules above the ring is denoted n^m and two rings of size *m* and *n* sharing a molecule is denoted $m{\cdot}n$.

TABLE 13: Minima Found on the $(HF)_n$ Potential Energy Surfaces with $3 \le n \le 6$. First-Order Induction Energy Used

label	energy/kJ mol^{-1}	PG[a]	description	dipole/au
trimer				
3a	−54.694	C_{3h}(p)	3	0.000
3b	−29.231	C_{2v}(p)	2_d	0.876
tetramer				
4a	−95.015	C_{4h}(p)	4	0.000
4b	−68.949	C_s(p)	3_d	1.005
4c	−65.511	C_s(p)	3_a	1.159
pentamer				
5a	−126.204	C_1	5	0.002
5b	−107.458	C_s(p)	4_d	0 905
5c	−101.500	C_s(p)	4_a	0 797
5d	−95.872	C_{2v}(p)	3·3	0.532
5e	−82.471	C_s(p)	3_{da}	1.822
5f	−80.526	C_s(p)	3_{dd}	0.949
5g	−73.892	C_s(p)	3_{aa}	1.021
hexamer				
6a	−153.368	S_6	6(chair)	0.000
6b	−153.044	C_2	6(book)	0.001
6c	−138.846	C_1	5^1	0.702
6d	−138.016	C_1	5_d	0.879
6e	−131.015	C_s(p)	4·3	0.557
6f	−129.129	C_s(p)	4_{2d}	1.327
6g	−123.553	S_6	3 3	0.000
6h	−121.516	C_s(p)	4_{2a}	1.599
6i	−118.485	C_{2h}(p)	4_{dd}	0.000
6j	−118.069	C_1	4^1_d	1.503
6k	−117.433	C_s(p)	4_{dd}	1.243
6l	−115.376	C_s(p)	4_{da}	1.784
6m	−115.152	C_s(p)	4_{da}	1.003
6n	−110.616	C_s(p)	$3{\cdot}3_d$	0.635
6o	−106.895	C_s(p)	$3{\cdot}3_a$	0.607
6p	−106.052	C_s(p)	3_{a2d}	1.712
6q	−89.485	C_{3h}(p)	3_{ddd}	0.000

[a] (p) denotes planar structure.

Table 13 illustrates that the energetic ordering of the minima is principally dependent on the cyclic unit present. Quack et al.[49] have commented on a transition to nonplanarity within the cyclic minima beyond $n = 5$. Our results would seem to disagree, with the pentamer being the first nonplanar cyclic minimum. However, if we optimize the structure with the induction energy converged at each step, we find that the pentamer cyclic minimum becomes planar with C_{5h} symmetry, bringing us into agreement with the previously published results. For the pentamer, we searched for a 4^1 stationary point and found a transition state connecting two versions of the 4_d minimum. For the hexamer the two lowest minima are cyclic with similar energies. The more strongly bound is the S_6 chair form and the other is the C_2 book form. Both of these structures were reported by Redington,[41] and the chair form has also been found by Quack et al.,[49] using a potential that includes three-body terms in the energy. These and a number of other minima are nonplanar (e.g., 5^1 and 4^1_d). We investigated the apparent absence of 4_{aa} minima and found that optimizations starting from such structures collapsed to 4_{dd} or 4_{ad} minima. We have found no chain structures, where each nonterminal HF molecule acts as both proton donor and acceptor, among the minima, but have observed them as transition states mediating rearrangements in which cyclic units unfold and refold.

3.2.2. Pathways. In addition to the characterization of the minima, we have also investigated rearrangement mechanisms. The motivation behind this was to identify mechanisms which could produce significant tunneling splittings that might be observed spectroscopically. Our pathways, listed in Table 15, are characterized in terms of the two connected minima (min 1 and min 2), the energy of the transition state (E_{ts}), the two energy

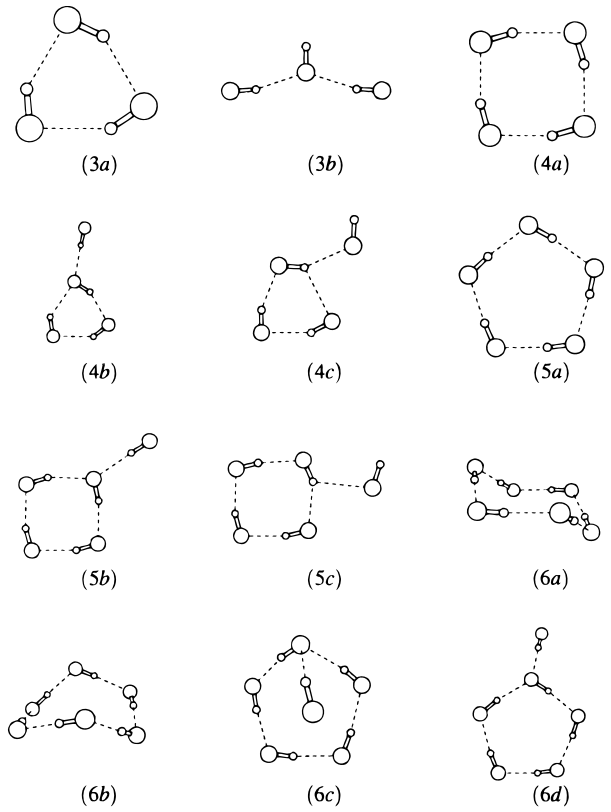

Figure 3. Low-lying $(HF)_n$ minima. See Table 13 for additional information.

TABLE 14: Comparison of the Binding Energies (kJ mol^{-1}) of the Cyclic Minima of $(HF)_n$ ($n = 3-6$) with Selected Previous Calculations. For the ASP-id potential, the Induction Energy Is Iterated to Convergence

		n			
ref	method	3	4	5	6
this work	ASP-id	−57.342	−103.525	−139.874	−170.288
19	MMC	−59.6	−104.5	−135.9	−166.9
99	ab initio	−64(2)	−116(3)	−158(4)	

barriers (ΔE_1 and ΔE_2), and the arc length along the EF reaction pathway (S), using the definition given by Wales.[68] The most important tunneling mechanisms are likely to be degenerate ($\Delta E_1 = \Delta E_2$) with small ΔE and S. We note for comparison that the values of these parameters for the dimer rearrangement calculated using ASP-id are 4.21 kJ mol^{-1} and 2.28 Å and that the experimental value for the tunneling splitting[88] in that case is 0.66 cm^{-1}, and bear in mind that the tunneling splitting is of the order $\exp(-S\sqrt{\mu\Delta E}/\hbar)$, where μ is a reduced mass. None of the paths found for the trimer satisfy these criteria. There are three degenerate rearrangements, the lowest barrier height being 13.845 kJ mol^{-1} and the corresponding value of S, 8.411 Å. We therefore expect that this rearrangement would yield a very small splitting. Several examples of D_{3h} symmetry transition states for degenerate rearrangement of the C_{3h} minimum have been reported.[53,96,99] These represent configurations for which each hydrogen atom is equidistant from two adjacent fluorine atoms in the ring, and the mechanism involves the concerted making and breaking of covalent bonds. At MP2 level of theory, the barrier height (including the zero-point energy contributions) was calculated to be about 65 kJ mol^{-1}.[99] Our potential is of rigid-body form, and hence we cannot model this type of process, but we note that the height of this barrier is considerably larger than that of our most feasible tunneling mechanism, although the width is probably much smaller. Quack et al. state[100] that $(HF)_5$ has "the lowest barrier to concerted hydrogen exchange in the oligomer series (35 kJ mol^{-1} at DZP MP2 level including harmonic zero-point correction").

TABLE 15: Selected Pathways on the $(HF)_n$ Potential Energy Surfaces with $3 \le n \le 6$[a] First-Order Induction Energy Used

min 1	ΔE_1	E_{ts}	PG	ΔE_2	min 2	S
trimer						
3a	13.845	−40.849	C_s	13.845	3a	8.411
3b	0.418	−28.813	C_s	25.881	3a	8.166
3a	28.406	−26.288	C_{2v}	28.406	3a	13.636
3a	28.415	−26.279	C_{2v}	28.415	3a	12.606
tetramer						
4a	26.253	−68.762	C_1	0.187	4b	5.315
4a	28.925	−66.090	C_s	28.925	4a	8.207
4a	29.555	−65.459	C_s	0.052	4c	5.770
4a	30.080	−64.934	C_s	30.080	4a	17.001
4b	5.796	−63.153	C_s	2.358	4c	3.039
4a	33.063	−61.952	C_s	33.063	4a	8.146
4a	49.416	−45.599	C_{2v}	49.416	4a	6.707
4a	49.885	−45.130	C_{2h}	49.885	4a	29.403
pentamer						
5b	1.197	−106.261	C_1	19.943	5a	6.782
5a	22.824	−103.380	C_s	22.824	5a	11.327
5b	5.930	−101.528	C_1	5.930	5b	12.424
5c	0.088	−101.412	C_s	6.046	5b	2.606
5c	1.231	−100.269	C_1	25.935	5a	5.487
5a	34.753	−91.451	C_s	34.753	5a	13.459
5d	4.491	−91.381	C_1	34.824	5a	11.013
5a	35.147	−91.057	C_1	4.815	5d	10.031
hexamer						
6b	0.019	−153.025	C_2	0.019	6b	2.071
6a	1.004	−152.365	C_1	0.680	6b	2.490
6a	2.533	−150.835	C_{6h}[b]	2.533	6b	2.526
6a	10.345	−143.024	C_1	10.021	6b	5.770
6c	1.099	−137.747	C_1	0.269	6d	5.168
6c	1.188	−137.658	C_1	15.387	6b	3.828
6c	1.429	−137.416	C_s	1.429	6c	3.109
6c	2.147	−136.698	C_1	2.147	6c	3.704
6b	20.056	−132.989	C_1	5.857	6c	7.739
6b	22.944	−130.100	C_s	22.944	6b	13.906

[a] Energies in kJ mol^{-1}. Arc lengths in angstroms. [b] This C_{6h} stationary point has Hessian index 3.

We find the lowest barriers for degenerate rearrangements of the tetramer and pentamer to be 28.925 and 5.930 kJ mol^{-1}, respectively, and the corresponding values of S are 8.207 and 12.424 Å. For the tetramer and pentamer we have found in each case a rearrangement involving a minimum based on the next smallest cyclic unit, with one additional HF molecule. These rearrangements exchange the role of the additional monomer from donor to acceptor, involve almost only the motion of that monomer, and look very similar to the dimer tunneling mechanism. However these rearrangements are not degenerate. The difference between the energies of the minima is 3.438 kJ mol^{-1} for the tetramer and 5.958 kJ mol^{-1} for the pentamer and the arc lengths are 3.039 and 2.606 Å. For the tetramer and pentamer, the barriers to concerted hydrogen exchange, calculated at MP2 level,[53] are 53.1 and 52.7 kJ mol^{-1}, respectively, again substantially larger than the corresponding values for our most feasible mechanisms.

The hexamer potential energy surface provides us with the first mechanisms which could lead to significant splittings. The lowest energy transition state found, at −153.025 kJ mol^{-1}, mediates a degenerate rearrangement involving the cyclic "book" minimum (6b). The barrier height is very small (0.019 kJ mol^{-1}) and the arc length is 2.07 Å. Both these values are smaller than the corresponding quantities on the dimer surface. However, this minimum has a very small dipole moment (≈0.001 au) and might prove difficult to detect in a

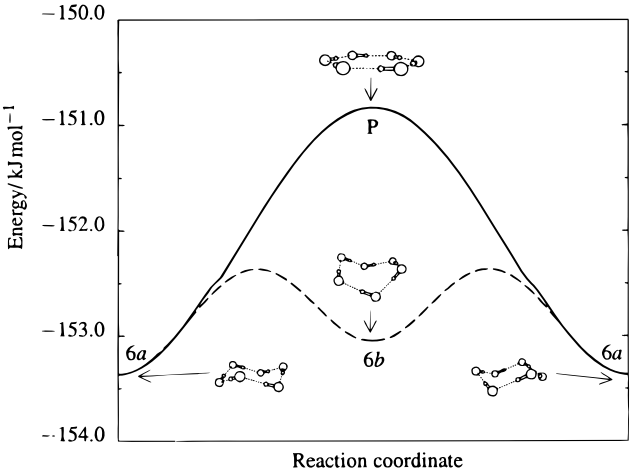

Figure 4. Degenerate rearrangement of the chair minimum (6a) of $(HF)_6$. The direct mechanism is via a planar, C_{6h} symmetry, index 3 stationary point (P); the multistep rearrangement proceeds via one of the book isomers (6b). See also Tables 13 and 15.

microwave experiment. Two further candidates involve the degenerate rearrangement of the 6c minimum, via transition states at 1.429 and 2.147 kJ mol^{-1} above the minimum with S = 3.109 and 3.704Å, respectively. We expect that these will lead to somewhat smaller splittings, but the minimum has a larger dipole moment (≈0.7 au). Also of interest is the planar, C_{6h} symmetry stationary point which causes inversion of the chair. This has Hessian index 3, so according to Murrell and Laidler[101] there must be a lower barrier to this rearrangement involving a "true transition state" (i.e., index 1). We believe that this is a multistep process, which proceeds via the transition state at −152.365 kJ mol^{-1} such that the lowest energy pathway linking the two isomers of the chair minimum involves passage through a book configuration (see Figure 4).

Another important experimental question is whether or not less stable local minima are populated. This would be sensitive to the rate of cooling, which if fast might favour the presence of such isomers.[100] For $n = 3-5$, the two lowest lying minima as found by ASP-id are of the types n and $(n-1)_d$. The barriers for conversion from the "tailed structures" to the cyclic global minima are found to be small—0.4, 0.2, and 1.2 kJ mol^{-1} for the trimer, tetramer, and pentamer, respectively. Previous work[98,102] suggests that the contributions from structural isomers will therefore be small, but their consideration may be necessary for the correct assignment of some spectra.[103,104]

3.3. Many-Body Contributions. In the pathway calculations, we have used a first-order approximation to the induction energy, because of computational time constraints. This accounts for three-body contributions, but not four-body or higher. For the complete analysis of these properties we must iterate the calculation of the induction energy to convergence, and we have reoptimized the minima. This sometimes results in a structure collapsing to a different minimum, and notably for the cyclic pentamer minimum, the fully optimized structure is planar, with C_{5h} symmetry, as opposed to the previously optimized C_1 structure.

The results for all minima are given in Table 16, and after reoptimization, the energetic ordering is the same as found with the first-order induction energy, with the exception of minima 6g and 6h. We note that for all cyclic minima, every component of each many-body contribution is attractive, which is true of none of the other minima. This helps to explain why the cyclic structures are particularly stable, even though their geometries would not appear to favor pairwise interactions as much as a three-dimensional structure might. This point has been raised before by Suhm,[98] who gives the relative stabilities of 5 and 4_d as an example, and describes the latter minimum as being "strongly disfavoured by the explicit three-body term".

TABLE 16: Decomposition of *n*-Body Contributions to the Energy for $(HF)_n$ Minima. Induction Energy Is Iterated to Convergence[a]

label	energy	2-body	3-body	4-body	5-body	6-body
trimer						
3a	−57.342	−50.067	−7.275			
3b	−29.464	−31.900	2.436			
tetramer						
4a	−103.525	−81.520	−20.029	−1.976		
4b	−72.411	−65.349	−7.019	−0.043		
4c	collapses to 4a					
pentamer						
5a	−139.874	−105.275	−30.310	−3.917	−0.373	
5b	−116.686	−95.680	−19.003	−2.018	0.015	
5c	−109.950	−89.230	−18.961	−1.780	0.021	
5d	−100.963	−90.219	−10.817	0.080	−0.007	
5e	−87.191	−78.367	−8.550	−0.288	0.014	
5f	collapses to 5b					
5g	−77.084	−71.734	−5.509	0.156	0.003	
hexamer						
6a	−170.288	−127.891	−36.761	−5.009	−0.588	−0.039
6b	−169.922	−127.492	−36.850	−4.959	−0.577	−0.044
6c	−152.546	−117.800	−31.088	−3.415	−0.251	0.008
6d	−152.304	−118.943	−29.073	−3.956	−0.335	0.003
6e	−141.099	−118.229	−21.201	−1.692	0.026	−0.002
6f	−139.811	−115.913	−21.794	−2.108	0.005	−0.001
6g	−129.689	−113.820	−15.861	0.068	−0.069	−0.008
6h	−130.659	−108.944	−19.980	−1.745	0.010	0.0003
6i	−127.925	−109.289	−16.895	−1.756	0.016	−0.001
6j	collapses to 6d					
6k	−127.002	−105.153	−19.748	−2.110	0.007	0.001
6l	−124.672	−104.344	−18.465	−1.883	0.018	0.002
6m	−124.481	−103.907	−18.733	−1.884	0.043	0.0002
6n	−116.659	−105.429	−11.320	0.108	−0.016	−0.001
6o	−112.499	−101.885	−10.641	0.025	0.002	−0.0007
6p	collapses to 6c					
6q	−92.530	−91.646	−1.571	0.751	−0.062	−0.002

[a] Energy in kJ mol^{-1}.

If we consider the highest order many-body term for the lowest energy structures from the trimer to the hexamer, they contribute respectively 12.7%, 1.91%, 0.266%, and 0.0230%, indicating that the many-body series is converging quite rapidly. Also, higher order terms than the three-body are very small, as found in previous work,[49] justifying the use of the "1+2+3 body" potential which accounts only for the 1-D, 6-D, and 12-D surfaces of the monomers, dimers, and trimers in HF clusters larger than the trimer.

We can also infer from Table 16 that for the noncyclic structures, the many-body contributions are mainly mediated by the cyclic unit present. For example, the tetramer minimum at −72.411 kJ mol^{-1} is based on the cyclic trimer. We therefore expect the three-body energy to be similar to that of minimum 3a (−7.019 vs −7.275 kJ mol^{-1}) and the four-body term to be small (0.043 kJ mol^{-1}). In fact for each noncyclic minimum, the highest order n-body term is much smaller than that for the cyclic minimum. Similar comparisons can be made for each of the tabulated minima, and the fact that the many-body terms for the cyclic structures are always attractive, coupled with the fact that such structures represent "saturated" hydrogen-bonded networks, means that, for HF clusters up to and including the pentamer, no three-dimensional minima analogous to those found in small water clusters have been found. We do expect some maximum number of molecules above which ring structures will not be favored, but we believe that it lies beyond $(HF)_6$. In preliminary searches of the $(HF)_7$ potential energy

surface, the two lowest minima found are chair- and book like cyclic structures at −179.72 and −179.25 kJ mol^{-1}. The next lowest lying structure is at −169.24 kJ mol^{-1} and is based on a cyclic hexamer with an HF molecule above the ring—6^1 using our notation.

4. Conclusions

We have described the construction of two new HF anisotropic site potentials ASP and ASP-id using monomer properties and intermolecular perturbation theory calculations, the total interaction energy being broken down into separate independent terms corresponding to definite physical interactions. Of the two, ASP is less satisfactory due to the lack of anisotropy in the damping of the dispersion energy. IMPT calculations show that the one-site dispersion model yields significantly different values, and since the dispersion at long range should be correct, we can attribute the deficiencies to the damping. The atom−atom dispersion model overcomes this problem to some extent, though it is not as good at long range. Also the repulsion energy computed here does not include correlation effects explicitly, and previous calculations[105,106] indicate that the repulsion energy can increase by 10% or so when correlation is included.

The dimer minimum energy structures predicted by our models are in quite good agreement with high level ab initio supermolecule calculations and with the experimental data available. The ASP-id model predicts with accuracy the geometries and energetics of the most important stationary points on the surface, and the barrier height for the tunneling motion is well reproduced. We also calculate the second virial coefficient for each potential, although at present there is no reliable experimental data for comparison. For this property we find that quantum corrections make a significant contribution, especially at low temperature, and cannot be omitted. We have extended the use of ASP-id to larger HF clusters, from the trimer to the hexamer, characterizing minima and rearrangement mechanisms. We find that cyclic structures dominate the minima and attribute this to the always favorable many-body interactions coupled with fact that the number of hydrogen bonds is optimal. From the analysis of barrier heights and widths we have found no rearrangement mechanisms for the trimer to the pentamer which are likely to produce significant tunneling splittings, but several potentially important tunneling mechanisms have been found for the hexamer.

In potentials like these, constructed from separate terms, corresponding to physically distinct interactions, each term has associated uncertainties, but in the present case, the biggest failure of the model seems to be the description of the dispersion energy at short range. Better potentials also require a more accurate description of the repulsion, taking electron correlation effects into account.

Acknowledgment. E.M.C.L. thanks the Theoretical Chemistry Group of the University of Santiago de Compostela for support for this work. M.P.H. and A.J.S. acknowledge financial support from the EPSRC. We thank Dr. Jon Gregory for providing us with his rigid-body diffusion Monte Carlo code.

References and Notes

(1) Dyke, T. R.; Howard, B. J.; Klemperer, W. *J. Chem. Phys.* **1972**, *56*, 2442.
(2) Howard, B. J.; Dyke, T. R.; Klemperer, W. *J. Chem. Phys.* **1984**, *81*, 5417.
(3) Gutowsky, H. S.; Chuang, C.; Keen, J. D.; Klots, T. D.; Emilsson, T. *J. Chem. Phys.* **1985**, *83*, 2070.
(4) Lafferty, W. J.; Suenram, R. D.; Looms, F. J. *J. Mol. Spectrosc.* **1987**, *123*, 434.
(5) Pine, A. S.; Lafferty, W. J. *J. Chem. Phys.* **1983**, *78*, 2154.
(6) Pine, A. S.; Lafferty, W. J.; Howard, B. J. *J. Chem. Phys.* **1984**, *81*, 2939.
(7) Pine, A. S.; Howard, B. J. *J. Chem. Phys.* **1986**, *84*, 590.
(8) Puttkamer, K. v.; Quack, M. *Mol. Phys.* **1987**, *62*, 1047.
(9) Quack, M.; Suhm, M. A. *Chem. Phys. Lett.* **1990**, *171*, 517.
(10) Bohac, E. J.; Marshall, M. D.; Miller, R. E. *J. Chem. Phys.* **1992**, *96*, 6681.
(11) Klopper, W.; Quack, M.; Suhm, M. A. *Chem. Phys. Lett.* **1996**, *261*, 35.
(12) Anderson, D. T.; Davis, S.; Nesbitt, D. J. *J. Chem. Phys.* **1996**, *105*, 4488.
(13) Peterson, K. A.; Dunning, T. H. *J. Chem. Phys.* **1995**, *102*, 2032.
(14) Novoa, J. J.; Planas, M.; Whangbo, M. *Chem. Phys. Lett.* **1994**, *225*, 240.
(15) Racine, S. C.; Davidson, E. R. *J. Phys. Chem.* **1993**, *97*, 6367.
(16) Del Bene, J. E. *Int. J. Quantum. Chem. Symp.* **1992**, *26*, 527.
(17) Quack, M.; Suhm, M. A. *J. Chem. Phys.* **1991**, *95*, 28.
(18) Rybak, S.; Jeziorski, B.; Szalewicz, K. *J. Chem. Phys.* **1991**, *95*, 6576.
(19) Dykstra, C. E. *J. Phys. Chem.* **1990**, *94*, 180.
(20) Jensen, P.; Bunker, P. R.; Karpfen, A.; Kofranek, M.; Lischka, H. *J. Chem. Phys.* **1990**, *93*, 6266.
(21) Bunker, P. R.; Jensen, P.; Karpfen, A.; Kofranek, M.; Lischka, H. *J. Chem. Phys.* **1990**, *92*, 7432.
(22) Bunker, P. R.; Carrington, Jr., T.; Gomez, P. C.; Marshall, M. D.; Kofranek, M.; Lischka, H.; Karpfen, A. *J. Chem. Phys.* **1989**, *91*, 5154.
(23) Bunker, P. R.; Kofranek, M.; Lischka, H.; Karpfen, A. *J. Chem. Phys.* **1988**, *89*, 3002.
(24) Kofranek, M.; Lischka, H.; Karpfen, A. *Chem. Phys.* **1988**, *121*, 137.
(25) Frisch, M. J.; Del Bene, J. E.; Binkley, J. S.; Schaefer, H. F., III, *J. Chem. Phys.* **1986**, *84*, 2279.
(26) Schwenke, D. W.; Truhlar, D. G. *J. Chem. Phys.* **1988**, *88*, 4800.
(27) Zhang, D. H.; Zhang, J. Z. H. *J. Chem. Phys.* **1993**, *99*, 6624.
(28) Zhang, D. H.; Wu, Q.; Zhang, J. Z. H.; von Dirke, M.; Bačić, Z. *J. Chem. Phys.* **1995**, *102*, 2315.
(29) Wu, Q.; Zhang, D. H.; Zhang, J. Z. H. *J. Chem. Phys.* **1995**, *103*, 2548.
(30) Kendall, R. A.; Dunning, T. H.; Harrison, R. J. *J. Chem. Phys.* **1992**, *96*, 6796.
(31) Quack, M.; Suhm, M. A. *Theor. Chim. Acta.* **1996**, *93*, 61.
(32) van Duijneveldt, F. B.; van Duijneveldt-van de Rijdt, J. G. C. M.; van Lenthe, J. H. *Chem. Rev.* **1994**, *94*, 1873.
(33) Chalasiński, G.; Gutowski, M. *Chem. Rev.* **1988**, *88*, 943.
(34) Jeziorski, B.; Moszynski, R.; Szalewicz, K. *Chem. Rev.* **1994**, *94*, 1887.
(35) Boys, S. F.; Bernardi, F. *Mol. Phys.* **1970**, *19*, 553.
(36) Hayes, I. C.; Stone, A. J. *Mol. Phys.* **1984**, *S3*, 69.
(37) Hayes, I. C.; Stone, A. J. *Mol. Phys.* **1984**, *53*, 83.
(38) Millot, C.; Stone, A. J. *Mol. Phys.* **1992**, *77*, 439.
(39) Stone, A. J.; Price, S. L. *J. Phys. Chem.* **1988**, *92*, 3325.
(40) Rodger, P. M.; Stone, A. J.; Tildesley, D. J. *Mol. Phys.* **1988**, *63*, 173.
(41) Redington, R. L. *J. Chem. Phys.* **1981**, *75*, 4417.
(42) Redington, R. L. *J. Phys. Chem.* **1982**, *86*, 552.
(43) Wilkins, R. L. *J. Chem. Phys.* **1977**, *67*, 5838.
(44) Jorgensen, W. L.; Cournoyer, M. E. *J. Am. Chem. Soc.* **1978**, *100*, 4942.
(45) Klein, M. L.; McDonald, I. R.; O'Shea, S. F. *J. Chem. Phys.* **1978**, *69*, 63.
(46) Poulsen, L. L.; Billing, G. D.; Steinfeld, J. I. *J. Chem. Phys.* **1978**, *68*, 5121.
(47) Jorgensen, W. L. *J. Chem. Phys.* **1979**, *70*, 5888.
(48) Klein, M. L.; McDonald, I. R. *J. Chem. Phys.* **1979**, *71*, 298.
(49) Quack, M.; Stohner, J.; Suhm, M. A. *J. Mol. Struct.* **1993**, *294*, 33.
(50) Liu, S.; Michael, D. W.; Dykstra, C. E.; Lisy, J. M. *J. Chem. Phys.* **1986**, *84*, 5032.
(51) Panas, I. *Chem. Phys. Lett.* **1993**, *216*, 173.
(52) Karpfen, A.; Yanovitskii, O. *J. Mol. Struct. (THEOCHEM)* **1994**, *120*, 211.
(53) Liedl, K. R.; Kroemer, R. T.; Rode, B. M. *Chem. Phys. Lett.* **1995**, *246*, 455.
(54) Cioslowski, J. *Theor. Chim. Acta.* **1990**, *77*, 253.
(55) Karpfen, A.; Yanovitskii, O. *J. Mol. Struct. (THEOCHEM)* **1994**, *113*, 81.
(56) Sadlej, A. J. *Theor. Chim. Acta.* **1991**, *79*, 123.
(57) Møller, C. M.; Plesset, M. S. *Phys. Rev.* **1934**, *46*, 618.
(58) Stone, A. J. *Chem. Phys. Lett.* **1993**, *211*, 101.

(59) Amos, R. D.; Rice, J. E., CADPAC6: *The Cambridge Analytical Derivatives Package*, Issue 6; University of Cambridge: Cambridge, 1995.
(60) Stone, A. J.; Alderton, M. *Mol. Phys.* **1985**, *56*, 1047.
(61) Stone, A. J. *Chem. Phys. Lett.* **1981**, *83*, 233.
(62) Rijks, W.; Wormer, P. E. S. *J. Chem. Phys.* **1989**, *90*, 6507.
(63) Rijks, W.; Wormer, P. E. S. *J. Chem. Phys.* **1990**, *92*, 5754.
(64) Hettema, H. 1995. Personal Communication.
(65) Tang, K. T.; Toennies, J. P. *J. Chem. Phys.* **1984**, *80*, 3726.
(66) Stone, A. J.; Dullweber, A.; Hodges, M. P.; Popelier, P. L. A.; Wales, D. J. ORIENT: *A program for studying interactions between molecules*, Version 3.2; University of Cambridge; Cambridge, 1995 (available at http://fandango.ch.cam.ac.uk.).
(67) Cerjan, C. J.; Miller, W. H. *J. Chem. Phys.* **1981**, *75*, 2800.
(68) Wales, D. J. *J. Chem. Phys.* **1994**, *101*, 3750.
(69) Stone, A. J. *The Theory of Intermolecular Forces;* Oxford University Press: Oxford, 1996.
(70) Huber, K. P.; Herzberg, G. *Molecular Spectra and Molecular Structure IV. Constants of Diatomic Molecules*; Van Nostrand: New York, 1979.
(71) Bass, S. M.; De Leon, R. L.; Muenter, J. S. *J. Chem. Phys.* **1987**, *86*, 4305.
(72) De Leeuw, W. H.; Dymanus, A. J. *J. Mol. Spectrosc.* **1973**, *48*, 427.
(73) Amos, R. D. *Chem. Phys. Lett.* **1982**, *88*, 89.
(74) Stone, A. J. *Mol. Phys.* **1978**, *36*, 241.
(75) Price, S. L.; Stone, A. J.; Alderton, M. *Mol. Phys.* **1984**, *52*, 987.
(76) Mirsky, K. *Computing in Crystallography*; Delft University Press: Delft, 1978.
(77) Stone, A. J. *Chem. Phys. Lett.* **1989**, *155*, 102.
(78) Stone, A. J. *Chem. Phys. Lett.* **1989**, *155*, 111.
(79) Hodges, M. P.; Stone, A. J.; Xantheas, S. S. *J. Phys. Chem.* **1997**, *101*, 9163.
(80) Xantheas, S. S. *J. Chem. Phys.* **1994**, *100*, 7523.
(81) Xantheas, S. S. *Phys. Mag. B.* **1996**, *73*, 107.
(82) Xantheas, S. S. *J. Chem. Phys.* **1996**, *104*, 8821.
(83) Chalasiński, G.; Cybulski, S. M.; Szczęśniak, M. M.; Scheiner, S. *J. Chem. Phys.* **1989**, *91*, 7048.
(84) Szczęśniak, M. M.; Chalasinski, G. *J. Mol. Struct. (THEOCHEM)* **1992**, *93*, 37.
(85) Gregory, J. K.; Clary, D. C. *J. Chem. Phys.* **1995**, *103*, 8924.
(86) Axilrod, P. M.; Teller, E. *J. Chem. Phys.* **1943**, *11*, 299.
(87) Stone, A. J.; Buckingham, A. D.; Fowler, P. W. *J. Chem. Phys.* **1997**, *107*, 1030.
(88) Belov, S. P.; Karyakin, E. N.; Kozin, I. N.; Krupnov, A. F.; Polyansky, O. L.; Tretyakov, M. Y.; Zobov, N. F.; Suenram, R. D.; Lafferty, W. J. *J. Mol. Spectrosc.* **1990**, *141*, 204.
(89) Gray, C. G.; Gubbins, K. E. *Theory of Molecular Fluids;* Clarendon Press, Oxford, 1984; Vol. 1.
(90) Bosanac, S.; Brobjer, J. T.; Murrell, J. N. *Mol. Phys.* **1984**, *51*, 313.
(91) Vukalovich, M. P.; Trakhtengerts, M. S.; Spiridonov, G. A. *Heat Power Engineering. Washington* **1967**, *14*, 86.
(92) Vukalovich, M. P.; Traskhtengerts, M. S.; Spiridonov, G. A. *Teoploenergetika* **1967**, *14*, 65.
(93) Kell, G. S.; McLaurin, G. E.; Whalley, E. *J. Chem. Phys.* **1968**, *48*, 3805.
(94) Kell, G. S.; McLaurin, G. E.; Whalley, E. *Proc. R. Soc. London, Ser. A.* **1989**, *425*, 49.
(95) Millot, C.; Soetens, J. C.; Martins Costa, M. T. C.; Hodges, M. P.; Stone, A. J. *J. Phys. Chem.* **1998**, *102*, 754.
(96) Gaw, J. F.; Yamaguchi, Y.; Vincent, M. A.; Schaefer, H. F., III *J. Am. Chem. Soc.* **1984**, *106*, 3133.
(97) Suhm, M. A.; Nesbitt, D. J. *Chem. Soc. Rev.* **1995**, *24*, 45.
(98) Suhm, M. A. *Ber. Bunsen-Ges. Phys. Chem.* **1995**, *99*, 1159.
(99) Quack, M.; Suhm, M. A. *Conceptual Trends in Quantum Chemistry*; Calais, J.-L., Kryachko, E. S., Eds., Kluwer: Dordrecht, 1997; Vol. III, pp 417−465.
(100) Quack, M.; Schmitt, U.; Suhm, M. A. *Chem. Phys. Lett.* **1993**, *208*, 446.
(101) Murrell, J. N.; Laidler, K. J. *Trans. Faraday Soc.* **1968**, *64*, 371.
(102) Luckhaus, D.; Quack, M.; Schmitt, U.; Suhm, M. A. *Ber. Bunsen-Ges. Phys. Chem.* **1995**, *99*, 457.
(103) Huisken, F.; Kaloudis, M.; Kulcke, A.; Laush, C.; Lisy, J. M. *J. Chem. Phys.* **1995**, *103*, 5366.
(104) Huisken, F.; Tarakanova, E. G.; Vigasin, A. A.; Yukhnevich, G. V. *Chem. Phys. Lett.* **1995**, *245*, 319.
(105) Rijks, W.; Gerritsen, M.; Wormer, P. E. S. *Mol. Phys.* **1989**, *66*, 929.
(106) Stone, A. J. *Am. Inst. Phys., Conf. Proc.* **1991**, *239*, 3.
(107) Muenter, J. S. *J. Phys. Chem.* **1972**, *56*, 5409.
(108) Werner, H. J.; Meyer, W. *Mol. Phys.* **1976**, *31*, 855.